Free vibration of axially loaded thin-walled composite Timoshenko beams

Thuc Phuong Vo* and Jaehong Lee†

Department of Architectural Engineering, Sejong University
98 Kunja Dong, Kwangjin Ku, Seoul 143-747, Korea

(Dated: October 19, 2013)

Based on shear-deformable beam theory, free vibration of thin-walled composite Timoshenko beams with arbitrary lay-ups under a constant axial force is presented. This model accounts for all the structural coupling coming from material anisotropy. Governing equations for flexural-torsional-shearing coupled vibrations are derived from Hamilton's principle. The resulting coupling is referred to as sixfold coupled vibrations. A displacement-based one-dimensional finite element model is developed to solve the problem. Numerical results are obtained for thin-walled composite beams to investigate the effects of shear deformation, axial force, fiber angle, modulus ratio on the natural frequencies, corresponding vibration mode shapes and load-frequency interaction curves.

Keywords: Thin-walled composite Timoshenko beams; shear deformation; sixfold coupled vibrations; axial force.

1. INTRODUCTION

Fiber-reinforced plastics have been used over the past few decades in a variety of structures. Composites have many desirable characteristics, such as high ratio of stiffness and strength to weight, corrosion resistance and magnetic transparency. Thin-walled structural shapes made up of composite materials, which are usually produced by pultrusion, are being increasingly used in many civil, mechanical and aerospace engineering applications. However, it is well known that thin-walled composite structures might be under axial force when used in above applications and are very susceptible to flexural-torsional buckling and display complex vibrational behavior. Therefore, the accurate prediction of their stability limit state and dynamic characteristics is of the fundamental importance in the design of composite structures.

The theory of thin-walled open-section members made of isotropic materials was first developed by Vlasov [**?**] and Gjelsvik [**?**]. Since the early works of Bleich et al. [**?**] and Timoshenko et al. [**?**,**?**], the investigation into vibration of thin-walled beams under axial loads of these members has been carried out extensively. A tensile axial load is

*Present Address: Department of Engineering, University of Liverpool, Brownlow Street, Liverpool L69 3GQ, UK

†Professor, corresponding author. Tel.:+82-2-3408-3287; fax:+82-2-3408-3331

; Electronic address: jhlee@sejong.ac.kr

well-known to increase the natural frequencies, whereas a compressive axial load will decrease the natural frequencies of beam members. For thin-walled composite beams, with the presence of the additional coupling effects from material anisotropy, these members under axial force exhibit strong coupling. Therefore, their vibration characteristic becomes more complicated than isotropic material even for doubly symmetric cross-section. This problem has been studied analytically by using some numerical techniques. The finite element method has been widely used because of its versatility and **a large amount of work** was devoted **to obtain** the acceptable results. Bank and Kao [**?**] analyzed free and forced vibration of thin-walled fibre reinforced composite material beams by using the Timoshenko beam theory. Cortinez and Piovan [**?**] presented a theoretical model for the vibration and buckling analysis of thin-walled composite beams. Later, Machado and Cortinez [**?**] investigated the influence of the initial in-plane deformations, generated by the action of a static external loading, as well as the effect of shear flexibility on the dynamic behavior of bisymmetric thin-walled composite beams. In their research [**?**,**?**], the analysis was based on a geometrically non-linear theory and thin-walled composite beams for both open and closed cross-sections and the shear flexibility (bending, non-uniform warping) were incorporated. However, it was strictly valid for symmetric balanced laminates and especially orthotropic laminates. On the other hand, another effective method solving the dynamic problem of thin-walled composite beams is to derive the exact stiffness matrices based on the solution of differential equations. Most of those studies adopted an analytical method that required explicit expressions of exact displacement functions for governing equations. By using this method, several authors have investigated the free vibration characteristic of axially loaded thin-walled closed-section composite beams (Banerjee et al. [**?**-**?**] and Li et al.[**?**,**?**] and Kaya and Ozgumus [**?**]) but only a few applied for thin-walled open-section composite beams. Kim et al.[**?**,**?**] evaluated dynamic stiffness matrix for flexural-torsional, lateral buckling and free vibration analyses of mono-symmetric thin-walled composite beams. A literature survey on the subject has revealed that studies of free vibration of thin-walled composite Timoshenko beams with arbitrary lay-ups including the influences of axial force and shear deformation in a unitary manner are limited. This complicated problem is not well-investigated and there is a need for further studies.

In this paper, which is an extension of the authors' previous works [**?**-**?**], free vibration of axially loaded thin-walled composite Timoshenko beams with arbitrary lay-ups is presented. This model is based on the first-order shear-deformable beam theory, and accounts for all the structural coupling coming from the material anisotropy. The seven governing differential equations for flexural-torsional-shearing coupled vibrations are derived from the Hamilton's principle. Numerical results are obtained for thin-walled composite beams to investigate the effects of shear deformation, axial force, fiber angle, modulus ratio on the natural frequencies and corresponding vibration

mode shapes as well as load-frequency interaction curves.

2. KINEMATICS

The theoretical developments presented in this paper require two sets of coordinate systems which are mutually interrelated. The first coordinate system is the orthogonal Cartesian coordinate system (x, y, z), for which the x and y axes lie in the plane of the cross section and the z axis parallel to the longitudinal axis of the beam. The second coordinate system is the local plate coordinate (n, s, z) as shown in Fig.**??**, wherein the n axis is normal to the middle surface of a plate element, the s axis is tangent to the middle surface and is directed along the contour line of the cross section. The (n, s, z) and (x, y, z) coordinate systems are related through an angle of orientation θ. As defined in Fig.**??** a point P, called the pole, is placed at an arbitrary point x_p, y_p. A line through P parallel to the z axis is called the pole axis.

To derive the analytical model for a thin-walled composite beam, the following assumptions are made:

1. The contour of the thin wall does not deform in its own plane.
2. Transverse shear strains $\gamma^{\circ}_{xz}, \gamma^{\circ}_{yz}$ and warping shear γ°_{ω} are incorporated. It is assumed that they are uniform over the cross-sections.
3. Each laminate is thin and perfectly bonded.
4. Local buckling is not considered.

According to assumption 1, the midsurface displacement components $\bar{u}, \bar{v}$ at a point A in the contour coordinate system can be expressed in terms of a displacements U, V of the pole P in the x, y directions, respectively, and the rotation angle Φ about the pole axis

$$\bar{u}(s,z) = U(z)\sin\theta(s) - V(z)\cos\theta(s) - \Phi(z)q(s) \tag{1a}$$

$$\bar{v}(s,z) = U(z)\cos\theta(s) + V(z)\sin\theta(s) + \Phi(z)r(s) \tag{1b}$$

These equations apply to the whole contour. For each element of middle surface, the midsurface shear strains in the contour can be expressed with respect to the transverse shear and warping shear strains.

$$\bar{\gamma}_{nz}(s,z) = \gamma^{\circ}_{xz}(z)\sin\theta(s) - \gamma^{\circ}_{yz}(z)\cos\theta(s) - \gamma^{\circ}_{\omega}(z)q(s) \tag{2a}$$

$$\bar{\gamma}_{sz}(s,z) = \gamma^{\circ}_{xz}(z)\cos\theta(s) + \gamma^{\circ}_{yz}(z)\sin\theta(s) + \gamma^{\circ}_{\omega}(z)r(s) \tag{2b}$$

Further, it is assumed that midsurface shear strain in $s-n$ direction is zero ($\bar{\gamma}_{sn}=0$). From the definition of the shear strain, $\bar{\gamma}_{sz}=0$ can also be given for each element of middle surface as

$$\bar{\gamma}_{sz}(s,z)=\frac{\partial\bar{v}}{\partial z}+\frac{\partial\bar{w}}{\partial s} \tag{3}$$

After substituting $\bar{v}$ from Eq.(??) into Eq.(??), the out-of-plane shell displacement $\bar{w}$ can be integrated with respect to s from the origin to an arbitrary point on the contour

$$\bar{w}(s,z) \;=\; W(z)+\Psi_y(z)x(s)+\Psi_x(z)y(s)+\Psi_\omega(z)\omega(s) \tag{4}$$

where Ψ_x,Ψ_y and Ψ_ω represent rotations of the cross section with respect to x,y and ω, respectively, given by

$$\Psi_y \;=\; \gamma^{\circ}_{xz}(z)-U' \tag{5a}$$

$$\Psi_x \;=\; \gamma^{\circ}_{yz}(z)-V' \tag{5b}$$

$$\Psi_\omega \;=\; \gamma^{\circ}_{\omega}(z)-\Phi' \tag{5c}$$

When the transverse shear effect is ignored, Eq.(**??**) degenerates to $\Psi_y=-U'$, $\Psi_x=-V'$ and $\Psi_\omega=-\Phi'$. As a result, the number of unknown variables reduces to four leading to the Euler-Bernoulli beam model. The prime ($'$) is used to indicate differentiation with respect to z; and ω is the so-called sectorial coordinate or warping function given by

$$\omega(s) \;=\; \int_{s_\circ}^{s} r(s)ds \tag{6}$$

The displacement components u,v,w representing the deformation of any generic point on the profile section are given with respect to the midsurface displacements $\bar{u},\bar{v},\bar{w}$ by assuming the first order variation of inplane displacements v, w through the thickness of the contour as

$$u(s,z,n) \;=\; \bar{u}(s,z) \tag{7a}$$

$$v(s,z,n) \;=\; \bar{v}(s,z)+n\bar{\psi}_s(s,z) \tag{7b}$$

$$w(s,z,n) \;=\; \bar{w}(s,z)+n\bar{\psi}_z(s,z) \tag{7c}$$

where, $\bar{\psi}_s$ and $\bar{\psi}_z$ denote the rotations of a transverse normal about the z and s axis, respectively. The function $\bar{\psi}_z$ can be determined by considering the shear strains γ_{nz} at midsurface

$$\gamma_{nz}(s,z)=\frac{\partial w}{\partial n}+\frac{\partial u}{\partial z}=\bar{\psi}_z+\frac{\partial\bar{u}}{\partial z} \tag{8}$$

By substituting Eqs.(**??**), (**??**) and (**??**) into Eq.(**??**), the function $\bar{\psi}_z$ can be written as

$$\bar{\psi}_z=\Psi_y\sin\theta-\Psi_x\cos\theta-\Psi_\omega q \tag{9}$$

Similarly, using the assumption that the shear strain γ_{sn} should vanish at midsurface, the function $\bar{\psi}_s$ can be obtained

$$\bar{\psi}_s = -\frac{\partial \bar{u}}{\partial s} \tag{10}$$

The non-zero strains associated with the small-displacement theory of elasticity are given by

$$\epsilon_z(s,z,n) = \frac{\partial w}{\partial z} = \bar{\epsilon}_z(s,z) + n\bar{\kappa}_z(s,z) \tag{11a}$$

$$\gamma_{sz}(s,z,n) = \frac{\partial w}{\partial s} + \frac{\partial v}{\partial z} = \bar{\gamma}_{sz}(s,z) + n\bar{\kappa}_{sz}(s,z) \tag{11b}$$

$$\gamma_{nz}(s,z,n) = \frac{\partial w}{\partial n} + \frac{\partial u}{\partial z} = \bar{\gamma}_{nz}(s,z) \tag{11c}$$

where

$$\bar{\epsilon}_z = \frac{\partial \bar{w}}{\partial z} = \epsilon_z^\circ + x\kappa_y + y\kappa_x + \omega\kappa_\omega \tag{12a}$$

$$\bar{\kappa}_z = \frac{\partial \bar{\psi}_z}{\partial z} = \kappa_y \sin\theta - \kappa_x \cos\theta - \kappa_\omega q \tag{12b}$$

$$\bar{\kappa}_{sz} = \frac{\partial \bar{\psi}_z}{\partial s} + \frac{\partial \bar{\psi}_s}{\partial z} = \kappa_{sz} \tag{12c}$$

The resulting strains can be obtained from Eqs.(**??**) and (**??**) as

$$\epsilon_z = \epsilon_z^\circ + (x + n\sin\theta)\kappa_y + (y - n\cos\theta)\kappa_x + (\omega - nq)\kappa_\omega \tag{13a}$$

$$\gamma_{sz} = \gamma_{xz}^\circ \cos\theta + \gamma_{yz}^\circ \sin\theta + \gamma_\omega^\circ r + n\kappa_{sz} \tag{13b}$$

$$\gamma_{nz} = \gamma_{xz}^\circ \sin\theta - \gamma_{yz}^\circ \cos\theta - \gamma_\omega^\circ q \tag{13c}$$

where $\epsilon_z^\circ, \kappa_x, \kappa_y, \kappa_\omega$ and κ_{sz} are axial strain, biaxial curvatures in the x and y direction, warping curvature with respect to the shear center, and twisting curvature in the beam, respectively defined as

$$\epsilon_z^\circ = W' \tag{14a}$$

$$\kappa_x = \Psi_x' \tag{14b}$$

$$\kappa_y = \Psi_y' \tag{14c}$$

$$\kappa_\omega = \Psi_\omega' \tag{14d}$$

$$\kappa_{sz} = \Phi' - \Psi_\omega \tag{14e}$$

3. VARIATIONAL FORMULATION

The total potential energy of the system can be stated, in its buckled shape, as

$$\Pi = \mathcal{U} + \mathcal{V} \tag{15}$$

where $\mathcal{U}$ is the strain energy

$$\mathcal{U} = \frac{1}{2}\int_v (\sigma_z\epsilon_z + \sigma_{sz}\gamma_{sz} + \sigma_{nz}\gamma_{nz})dv \tag{16}$$

After substituting Eq.(**??**) into Eq.(**??**)

$$\begin{aligned}\mathcal{U} &= \frac{1}{2}\int_v \Big\{\sigma_z\Big[\epsilon_z^\circ + (x + n\sin\theta)\kappa_y + (y - n\cos\theta)\kappa_x + (\omega - nq)\kappa_\omega\Big] \\ &+ \sigma_{sz}\Big[\gamma_{xz}^\circ\cos\theta + \gamma_{yz}^\circ\sin\theta + \gamma_\omega^\circ r + n\kappa_{sz}\Big] + \sigma_{nz}\Big[\gamma_{xz}^\circ\sin\theta - \gamma_{yz}^\circ\cos\theta - \gamma_\omega^\circ q\Big]\Big\}dv\end{aligned} \tag{17}$$

The variation of strain energy, Eq.(**??**), can be stated as

$$\delta\mathcal{U} = \int_0^l (N_z\delta\epsilon_z + M_y\delta\kappa_y + M_x\delta\kappa_x + M_\omega\delta\kappa_\omega + V_x\delta\gamma_{xz}^\circ + V_y\delta\gamma_{yz}^\circ + T\delta\gamma_\omega^\circ + M_t\delta\kappa_{sz})dz \tag{18}$$

where $N_z, M_x, M_y, M_\omega, V_x, V_y, T, M_t$ are axial force, bending moments in the x- and y-directions, warping moment (bimoment), and torsional moment with respect to the centroid, respectively, defined by integrating over the cross-sectional area A as

$$N_z = \int_A \sigma_z dsdn \tag{19a}$$

$$M_y = \int_A \sigma_z(x + n\sin\theta)dsdn \tag{19b}$$

$$M_x = \int_A \sigma_z(y - n\cos\theta)dsdn \tag{19c}$$

$$M_\omega = \int_A \sigma_z(\omega - nq)dsdn \tag{19d}$$

$$V_x = \int_A (\sigma_{sz}\cos\theta + \sigma_{nz}\sin\theta)dsdn \tag{19e}$$

$$V_y = \int_A (\sigma_{sz}\sin\theta - \sigma_{nz}\cos\theta)dsdn \tag{19f}$$

$$T = \int_A (\sigma_{sz}r + \sigma_{nz}q)dsdn \tag{19g}$$

$$M_t = \int_A \sigma_{sz}ndsdn \tag{19h}$$

The potential of in-plane loads $\mathcal{V}$ due to transverse deflection

$$\mathcal{V} = \frac{1}{2}\int_v \overline{\sigma}_z^0\Big[(u')^2 + (v')^2\Big]dv \tag{20}$$

where $\overline{\sigma}_z^0$ is the averaged constant in-plane edge axial stress, defined by $\overline{\sigma}_z^0 = P_0/A$. The variation of the potential of in-plane loads at the centroid is expressed by substituting the assumed displacement field into Eq.(**??**) as

$$\begin{aligned}\delta\mathcal{V} &= \int_v \frac{P_0}{A}\Big[U'\delta U' + V'\delta V' + (q^2 + r^2 + 2rn + n^2)\Phi'\delta\Phi' + (\Phi'\delta U' + U'\delta\Phi')\big[n\cos\theta - (y - y_p)\big] \\ &+ (\Phi'\delta V' + V'\delta\Phi')\big[n\cos\theta + (x - x_p)\big]\Big]dv\end{aligned} \tag{21}$$

The kinetic energy of the system is given by

$$\mathcal{T} \;=\; \frac{1}{2}\int_v \rho(\dot{u}^2+\dot{v}^2+\dot{w}^2)dv \tag{22}$$

where ρ is a density.

The variation of the kinetic energy is expressed by substituting the assumed displacement field into Eq.(**??**) as

$$\begin{aligned}
\delta\mathcal{T} \;=\; & \int_v \rho\Bigg\{ \delta\dot{W}\Big[\dot{W}+\dot{\Psi}_x(y-n\cos\theta)+\dot{\Psi}_y(x+n\sin\theta)+\dot{\Psi_\omega}(\omega-nq)\Big] \\
& +\; \delta\dot{U}\Big[\dot{U}+\dot{\Phi}\Big[n\cos\theta-(y-y_p)\Big]\Big]+\delta\dot{V}\Big[m_0\dot{V}+\dot{\Phi}\Big[n\sin\theta+(x-x_p)\Big]\Big] \\
& +\; \delta\dot{\Phi}\dot{\Phi}\Big[\dot{U}\Big[n\cos\theta-(y-y_p)\Big]+\dot{V}\Big[n\sin\theta+(x-x_p)\Big]+\dot{\Phi}(q^2+r^2+2rn+n^2)\Big] \\
& +\; \delta\dot{\Psi}_x\dot{\Psi}_x\Big[\dot{W}(y-n\cos\theta)+\dot{\Psi}_x(y-n\cos\theta)^2+\dot{\Psi}_y(x+n\sin\theta)(y-n\cos\theta)+\dot{\Psi}_\omega(y-n\cos\theta)(\omega-nq)\Big] \\
& +\; \delta\dot{\Psi}_y\dot{\Psi}_y\Big[\dot{W}(x+n\sin\theta)+\dot{\Psi}_x(x+n\sin\theta)(y-n\cos\theta)+\dot{\Psi}_y(x+n\sin\theta)^2+\dot{\Psi}_\omega(x+n\sin\theta)(\omega-nq)\Big] \\
& +\; \delta\dot{\Psi_\omega}\dot{\Psi}_\omega\Big[\dot{W}(\omega-nq)+\dot{\Psi}_x(y-n\cos\theta)(\omega-nq)+\dot{\Psi}_y(x+n\sin\theta)(\omega-nq)+\dot{\Psi}_\omega(\omega-nq)^2\Big]\Bigg\}dv
\end{aligned} \tag{23}$$

In order to derive the equations of motion, Hamilton's principle is used

$$\delta\int_{t_1}^{t_2}(\mathcal{T}-\Pi)dt \;=\; 0 \tag{24}$$

Substituting Eqs.(**??**), (**??**) and (**??**) into Eq.(**??**), the following weak statement is obtained

$$\begin{aligned}
0 \;=\; & \int_{t_1}^{t_2}\int_0^l \Big\{\delta\dot{W}\Big[m_0\dot{W}-m_c\dot{\Psi}_x+m_s\dot{\Psi}_y+(m_\omega-m_q)\dot{\Psi_\omega}\Big]+\delta\dot{U}\Big[m_0\dot{U}+(m_c+y_pm_0)\dot{\Phi}\Big] \\
& +\; \delta\dot{V}\Big[m_0\dot{V}+(m_s-x_pm_0)\dot{\Phi}\Big]+\delta\dot{\Phi}\Big[(m_c+y_pm_0)\dot{U}+(m_s-x_pm_0)\dot{V}+(m_p+m_2+2m_r)\dot{\Phi}\Big] \\
& +\; \delta\dot{\Psi}_x\Big[-m_c\dot{W}+(m_{y2}-2m_{yc}+m_{c2})\dot{\Psi}_x+(m_{xycs}-m_{cs})\dot{\Psi}_y+(m_{y\omega}-m_{y\omega qc}+m_{qc})\dot{\Psi}_\omega\Big] \\
& +\; \delta\dot{\Psi}_y\Big[m_s\dot{W}+(m_{xycs}-m_{cs})\dot{\Psi}_x+(m_{x2}+2m_{xs}+m_{s2})\dot{\Psi}_y+(m_{x\omega}+m_{x\omega qs}-m_{qs})\dot{\Psi}_\omega\Big] \\
& +\; \delta\dot{\Psi_\omega}\Big[(m_\omega-m_q)\dot{W}+(m_{y\omega}-m_{y\omega qc}+m_{qc})\dot{\Psi}_x+(m_{x\omega}+m_{x\omega qs}-m_{qs})\dot{\Psi}_y+(m_{\omega 2}-2m_{q\omega}+m_{q2})\dot{\Psi}_\omega\Big] \\
& -\; P_0\big[\delta U'(U'+\Phi' y_p)+\delta V'(V'-\Phi' x_p)+\delta\Phi'(\Phi'\frac{I_p}{A}+U'y_p-V'x_p)\big]-N_z\delta W' \\
& -\; M_y\delta\Psi_y'-M_x\delta\Psi_x'-M_\omega\delta\Psi_\omega'-V_x\delta(U'+\Psi_y)-V_y\delta(V'+\Psi_x)-T\delta(\Phi'-\Psi_\omega)-M_t\delta(\Phi'-\Psi_\omega)\Big\}dzdt
\end{aligned} \tag{25}$$

All the inertia coefficients in Eq.(**??**) are given in Ref.[**?**].

4. CONSTITUTIVE EQUATIONS

The constitutive equations of a k^{th} orthotropic lamina in the laminate co-ordinate system of section are given by

$$\left\{ \begin{array}{c} \sigma_z \\ \sigma_{sz} \end{array} \right\}^k = \left[\begin{array}{cc} \bar{Q}^*_{11} & \bar{Q}^*_{16} \\ \bar{Q}^*_{16} & \bar{Q}^*_{66} \end{array} \right]^k \left\{ \begin{array}{c} \epsilon_z \\ \gamma_{sz} \end{array} \right\} \tag{26}$$

where $\bar{Q}^*_{ij}$ are transformed reduced stiffnesses. The transformed reduced stiffnesses can be calculated from the transformed stiffnesses based on the plane stress ($\sigma_s = 0$) and plane strain ($\epsilon_s = 0$) assumption. More detailed explanation can be found in Ref.[**?**].

The constitutive relation for out-of-plane stress and strain is given by

$$\sigma_{nz} = \bar{Q}_{55}\gamma_{nz} \tag{27}$$

The constitutive equations for bar forces and bar strains are obtained by using Eqs.(**??**), (**??**) and (**??**)

$$\left\{ \begin{array}{c} N_z \\ M_y \\ M_x \\ M_\omega \\ M_t \\ V_x \\ V_y \\ T \end{array} \right\} = \left[\begin{array}{cccccccc} E_{11} & E_{12} & E_{13} & E_{14} & E_{15} & E_{16} & E_{17} & E_{18} \\ & E_{22} & E_{23} & E_{24} & E_{25} & E_{26} & E_{27} & E_{28} \\ & & E_{33} & E_{34} & E_{35} & E_{36} & E_{37} & E_{38} \\ & & & E_{44} & E_{45} & E_{46} & E_{47} & E_{48} \\ & & & & E_{55} & E_{56} & E_{57} & E_{58} \\ & & & & & E_{66} & E_{67} & E_{68} \\ & & & & & & E_{77} & E_{78} \\ \text{sym.} & & & & & & & E_{88} \end{array} \right] \left\{ \begin{array}{c} \epsilon^\circ_z \\ \kappa_y \\ \kappa_x \\ \kappa_\omega \\ \kappa_{sz} \\ \gamma^\circ_{xz} \\ \gamma^\circ_{yz} \\ \gamma^\circ_\omega \end{array} \right\} \tag{28}$$

where E_{ij} are stiffnesses of thin-walled composite beams and given in Ref.[**?**].

5. EQUATIONS OF MOTION

The equations of motion of the present study can be obtained by integrating the derivatives of the varied quantities by parts and collecting the coefficients of $\delta W, \delta U, \delta V, \delta\Phi, \delta\Psi_y, \delta\Psi_x$ and $\delta\Psi_\omega$

$$N_z' = m_0\ddot{W} - m_c\ddot{\Psi}_x + m_s\ddot{\Psi}_y + (m_\omega - m_q)\ddot{\Psi}_\omega \tag{29a}$$

$$V_x' + P_0\big(U'' + \Phi'' y_p\big) = m_0\ddot{U} + (m_c + y_p m_0)\ddot{\Phi} \tag{29b}$$

$$V_y' + P_0\big(V'' - \Phi'' x_p\big) = m_0\ddot{V} + (m_s - x_p m_0)\ddot{\Phi} \tag{29c}$$

$$\begin{aligned} M_t' + T' + P_0\big(\Phi''\frac{I_p}{A} + U'' y_p - V'' x_p\big) &= (m_c - m_y + y_p m_0)\ddot{U} + (m_s - x_p m_0)\ddot{V} \\ &+ (m_p + m_2 + 2m_r)\ddot{\Phi} \end{aligned} \tag{29d}$$

$$\begin{aligned} M_y' - V_x &= m_s\ddot{W} + (m_{xycs} - m_{cs})\ddot{\Psi}_x + (m_{x2} + 2m_{xs} + m_{s2})\ddot{\Psi}_y \\ &+ (m_{x\omega} + m_{x\omega qs} - m_{qs})\ddot{\Psi}_\omega \end{aligned} \tag{29e}$$

$$\begin{aligned} M_x' - V_y &= -m_c\ddot{W} + (m_{y2} - 2m_{yc} + m_{c2})\ddot{\Psi}_x + (m_{xycs} - m_{cs})\ddot{\Psi}_y \\ &+ (m_{y\omega} - m_{y\omega qc} + m_{qc})\ddot{\Psi}_\omega \end{aligned} \tag{29f}$$

$$\begin{aligned} M_\omega' + M_t - T &= (m_\omega - m_q)\ddot{W} + (m_{y\omega} - m_{y\omega qc} + m_{qc})\ddot{\Psi}_x \\ &+ (m_{x\omega} + m_{x\omega qs} - m_{qs})\ddot{\Psi}_y \\ &+ (m_{\omega 2} - 2m_{q\omega} + m_{q2})\ddot{\Psi}_\omega \end{aligned} \tag{29g}$$

The natural boundary conditions are of the form

$$\delta W \ : \qquad W = \overline{W}_0 \quad \text{or} \quad N_z = P_0 \tag{30a}$$

$$\delta U \ : \qquad U = \overline{U}_0 \quad \text{or} \quad V_x = \overline{V}_{x_0} \tag{30b}$$

$$\delta V \ : \qquad V = \overline{V}_0 \quad \text{or} \quad V_y = \overline{V}_{y_0} \tag{30c}$$

$$\delta\Phi \ : \qquad \Phi = \overline{\Phi}_0 \quad \text{or} \quad T + M_t = \overline{T}_0 + \overline{M}_{t_0} \tag{30d}$$

$$\delta\Psi_y \ : \qquad \Psi_y = \overline{\Psi}_{y_0} \quad \text{or} \quad M_y = \overline{M}_{y_0} \tag{30e}$$

$$\delta\Psi_x \ : \qquad \Psi_x = \overline{\Psi}_{x_0} \quad \text{or} \quad M_x = \overline{M}_{x_0} \tag{30f}$$

$$\delta\Psi_\omega \ : \qquad \Psi_\omega = \overline{\Psi}_{\omega_0} \quad \text{or} \quad M_\omega = \overline{M}_{\omega_0} \tag{30g}$$

The 7^{th} denotes the warping restraint boundary condition. When the warping of the cross section is restrained, $\Psi_\omega = 0$ and when the warping is not restrained, $M_\omega = 0$.

Eq.(**??**) is most general form for free vibration of thin-walled composite Timoshenko beams under a constant axial force. For general anisotropic materials, the dependent variables, U, V, W, Φ, Ψ_x, Ψ_y and Ψ_ω are fully-coupled implying that the beam undergoes a coupled behavior involving bending, extension, twisting, transverse shearing, and warping. The resulting coupling is referred to as sixfold coupled vibrations. If all the coupling effects are neglected and cross section is symmetrical with respect to both x- and the y-axes, Eq.(**??**) can be simplified to the uncoupled differential equations as

$$(EA)_{com}W'' = \rho A\ddot{W} \tag{31a}$$

$$(GA_y)_{com}(U'' + \Psi_y') + P_0U'' = \rho A\ddot{U} \tag{31b}$$

$$(GA_x)_{com}(V'' + \Psi_x') + P_0V'' = \rho A\ddot{V} \tag{31c}$$

$$\Big[(GJ_1)_{com} + P_0\frac{I_p}{A}\Big]\Phi'' - (GJ_2)_{com}\Psi_\omega' = \rho I_p\ddot{\Phi} \tag{31d}$$

$$(EI_y)_{com}\Psi_y'' - (GA_y)_{com}(U' + \Psi_y) = \rho I_y\ddot{\Psi}_y \tag{31e}$$

$$(EI_x)_{com}\Psi_x'' - (GA_x)_{com}(V' + \Psi_x) = \rho I_x\ddot{\Psi}_x \tag{31f}$$

$$(EI_\omega)_{com}\Psi_\omega'' + (GJ_2)_{com}\Phi' - (GJ_1)_{com}\Psi_\omega = \rho I_\omega\ddot{\Psi}_\omega \tag{31g}$$

It is well known that the three distinct vibration mode, flexural vibration in the x- and y-direction and torsional vibration are identified in this case. From above equations, $(EA)_{com}$ represents axial rigidity, $(GA_x)_{com}$, $(GA_y)_{com}$ represent shear rigidities with respect to x and y axis, $(EI_x)_{com}$ and $(EI_y)_{com}$ represent flexural rigidities with respect to x- and y-axis, $(EI_\omega)_{com}$ represents warping rigidity, and $(GJ_1)_{com}$, $(GJ_2)_{com}$ represent torsional rigidities of thin-walled composite beams, respectively, written as

$$(EA)_{com} = E_{11} \tag{32a}$$

$$(EI_y)_{com} = E_{22} \tag{32b}$$

$$(EI_x)_{com} = E_{33} \tag{32c}$$

$$(EI_\omega)_{com} = E_{44} \tag{32d}$$

$$(GA_y)_{com} = E_{66} \tag{32e}$$

$$(GA_x)_{com} = E_{77} \tag{32f}$$

$$(GJ_1)_{com} = E_{55} + E_{88} \tag{32g}$$

$$(GJ_2)_{com} = E_{55} - E_{88} \tag{32h}$$

6. FINITE ELEMENT FORMULATION

The present theory for thin-walled composite Timoshenko beams described in the previous section is implemented via a one-dimensional displacement-based finite element method. The same interpolation function is used for all the translational and rotational displacements. Reduced integration of shear terms, that is, stiffness coefficients involving laminate stiffnesses ($E_{i,j}$, $i = 6..8, j = 6..8$) is used to avoid shear locking. The generalized displacements are expressed over each element as a combination of the one-dimensional Lagrange interpolation function $\widehat{\phi_j}$ associated with node j and the nodal values

$$W = \sum_{j=1}^{n} w_j \widehat{\phi_j} \tag{33a}$$

$$U = \sum_{j=1}^{n} u_j \widehat{\phi_j} \tag{33b}$$

$$V = \sum_{j=1}^{n} v_j \widehat{\phi_j} \tag{33c}$$

$$\Phi = \sum_{j=1}^{n} \phi_j \widehat{\phi_j} \tag{33d}$$

$$\Psi_y = \sum_{j=1}^{n} \psi_{yj} \widehat{\phi_j} \tag{33e}$$

$$\Psi_x = \sum_{j=1}^{n} \psi_{xj} \widehat{\phi_j} \tag{33f}$$

$$\Psi_\omega = \sum_{j=1}^{n} \psi_{\omega j} \widehat{\phi_j} \tag{33g}$$

where n is the number of nodes in an element and Lagrange interpolation function $\widehat{\phi_j}$ for linear, quadratic and cubic elements are available in the literature.

Substituting these expressions into the weak statement in Eq.(**??**), the finite element model of a typical element can be expressed as

$$([K] - P_0[G] - \omega^2[M])\{\Delta\} = \{0\} \tag{34}$$

where $[K], [G]$ and $[M]$ are the element stiffness matrix, the element geometric stiffness matrix and the element mass matrix, respectively. The explicit forms of them are given in Refs.[**?-?**].

In Eq.(**??**), $\{\Delta\}$ is the eigenvector of nodal displacements corresponding to an eigenvalue

$$\{\Delta\} = \{W\ U\ V\ \Phi\ \Psi_y\ \Psi_x\ \Psi_\omega\}^{\mathrm{T}} \tag{35}$$

7. NUMERICAL EXAMPLES

For verification purpose, the buckling behavior and free vibration of a cantilever symmetrically laminated mono-symmetric I-beam with length $l = 1$m under axial load at the centroid is considered. Following dimensions for the I-beam are used: the height, top and bottom flange widths are 50mm, 30mm and 50mm, respectively. The flanges and web are made of sixteen layers with each layer 0.13mm in thickness. All computations are carried out for the glass-epoxy materials with the following material properties: $E_1 = 53.78$GPa $, E_2 = 17.93$GPa $, G_{12} = G_{13} = 8.96$GPa $, G_{23} = 3.45$GPa $, \nu_{12} = 0.25$ $, \rho = 1968.9$kg/m^3. **In Table ??, the critical buckling loads are compared with numerical results of Kim and Shin [?], which is based on dynamic stiffness formulation and ABAQUS solution by using nine-noded shell element (S9R5). It is clear that the numerical solution using ABAQUS always underestimates the analytical solution except for** $[60/-60]_{4s}$ **lay-up. However, the buckling load of this case is overestimated approximate by 3%, which is an acceptable error**. Next, the flexural-torsional coupled vibration analysis of axially loaded cantilever beam is evaluated. The applied magnitude of axial force is given in Ref. [**?**], which corresponds to one half of buckling load of beam. The lowest four coupled natural frequencies with and without the axial force are presented in Table **??**. It reveals that the tension force has a stiffening effect while the compressive force has a softening effect on the natural frequencies of the beam. It can be seen from Tables **??** and **??** that the present results are in a good agreement with those by Kim and Shin [**?**].

In order to investigate the effects of axial force, fiber orientation and shear deformation on the natural frequencies and corresponding vibration mode shapes as well as load-frequency interaction curves, thin-walled composite I-beams with length $l = 3$m and various boundary conditions under axial load at the centroid are considered. The geometry and stacking sequences of I-section are shown in Fig.**??**, and the following engineering constants are used

$$E_1/E_2 = 25, G_{12}/E_2 = 0.6, G_{13} = G_{12} = G_{23}, \nu_{12} = 0.25 \tag{36}$$

For convenience, the following nondimensional buckling load and natural frequency are used

$$\overline{P} = \frac{P_0 l^2}{b_3^3 t E_2} \tag{37}$$

$$\overline{\omega} = \frac{\omega l^2}{b_3}\sqrt{\frac{\rho}{E_2}} \tag{38}$$

As a first example, a simply supported composite I-beam is considered. Stacking sequences of the flanges and web are angle-ply laminates $[\theta/-\theta]$, (Fig. **??**a). For this lay-up, all the coupling stiffnesses are zero, but E_{35} and E_{38}

do not vanish due to unsymmetric stacking sequence of the flanges and web. In Table **??**, effects of axial force and flexural-torsional coupling on the lowest four natural frequencies are inspected. This demonstrates again the well-known fact that a tensile force stiffens the beam and a compressive force softens the beam. The uncoupled solution, which neglects the coupling effects, is also given. The critical buckling loads agree completely with those of previous paper [**?**], as expected. Due to coupling stiffnesses, the uncoupled solution might not be accurate. However, as fiber angle increases, the coupling effects coming from the material anisotropy become negligible. It can be seen in Table **??** that for all cases of fiber angles, the lowest four natural frequencies by the coupled solution always correspond to the first flexural mode in x-direction, the the first torsional mode, the first flexural mode in y-direction and the second flexural mode in x-direction by the uncoupled solution, respectively. It is indicated that the uncoupled solution is sufficiently accurate for this lay-up. It can be explained partly by the typical normal mode shapes with fiber angle $\theta = 30^\circ$ for the case of axial compressive force ($\overline{P} = 0.5\overline{P}_{cr}$) in Fig.**??**. The mode shapes for other cases of axial force ($\overline{P} = 0$ and $\overline{P} = -0.5\overline{P}_{cr}$) are similar to the corresponding ones for the case of axial force ($\overline{P} = 0.5\overline{P}_{cr}$) and are not plotted, although there is a little difference between them. Three dimensional fiber-axial-frequency interaction diagram with respect to the fiber angle change is illustrated in Fig. **??**. Four groups of curves corresponding to $\omega_1, \omega_2, \omega_3$ and ω_4 are observed. It is interesting to see that two larger groups, $(\omega_3 - P_3)$ and $(\omega_4 - P_4)$, always intersect each other for all fiber angles. To investigate the effects of shear deformation on the load-frequency interaction curves, the stacking sequence at fiber angles $\theta = 0^\circ, 30^\circ$ and 60° is considered. The lowest four load-frequency interaction curves at these fiber angles are shown in Figs.**??**-**??**. These curves obtained from previous research [**?**] based on the classical beam theory are also displayed. It is obvious that the natural frequencies decrease with the increase of axial force, and the decrease becomes more quickly when the axial force is close to buckling loads. Shear effects are more pronounced with unidirectional fiber direction (Fig.**??**) and decrease as fiber angle increases (Figs.**??** and **??**). This trend can be explained that flexural stiffnesses decrease significantly with increasing fiber angle, and thus, the relative shear effects become smaller for the higher fiber angles. Figs.**??**-**??** also explain the duality between the flexural-torsional buckling loads and the natural frequencies.

To investigate the coupling and shear effects further, a clamped composite I-beam is performed. The bottom flange is considered as $[\theta_2]$, while the top flange and web are $[0/45]$, respectively (Fig.**??**b). For this lay-up, the coupling stiffnesses $E_{16}, E_{17}, E_{18}, E_{36}, E_{37}$ and E_{68} become no more negligibly small. Major effects of axial force and shear deformation on the natural frequencies are again seen in Table **??**. It is indicated that the solutions excluding shear effects remarkably underestimate the natural frequencies for all fiber angles. This implies that discarding shear effects

leads to an overprediction of the natural frequencies. The interaction diagram between the flexural-torsional buckling loads and natural frequencies by the coupled and uncoupled solution with the fiber angle $\theta = 0^\circ$ and 60° are displayed in Figs.**??** and **??**. Characteristic of load-frequency interaction curves is that the value of the axial force for which the natural frequencies vanish constitute the buckling loads. Thus, for $\theta = 60^\circ$, the first and second flexural-torsional bucklings occur at $\overline{P} = 2.861$ and 5.695. As a result, the lowest two branches vanish when $\overline{P}$ is slightly over $\overline{P} = 5.695$. As the axial force increases, two interaction curves $(w_3 - P_3)$ and $(w_4 - P_4)$ intersect at $\overline{P} = 9.413$, thus, after this value, the phenomenon of mode shifting for mode 3 and 4 can be observed. Finally, the third and fourth branch will also disappear when $\overline{P}$ is slightly over 10.790 and 15.641, respectively. The typical normal mode shapes corresponding to the lowest four natural frequencies with fiber angle $\theta = 30^\circ$ for the case of axial compressive force ($\overline{P} = 0.5\overline{P}_{cr}$) are illustrated in Fig.**??**. Relative measures of flexural displacements, torsional and shearing rotation show that when the beam is vibrating at the natural frequency belonging to the first and second mode exhibit fourfold coupled modes (flexural vibration in the x-direction, torsional and corresponding shearing vibration), whereas, third and fourth mode display sixfold coupled modes (flexural mode in the x-, y-direction, torsional mode and corresponding shearing vibration). This fact explains as the fiber angle changes, for lower span-to-height ratio, the uncoupled solution disagree with coupled solution as anisotropy of the beam gets higher. That is, the uncoupled solution is no longer valid for unsymmetrically laminated beams, and sixfold flexural-torsional-shearing coupled vibrations should be considered even for a doubly symmetric cross-section.

Finally, the effects of modulus ratio (E_1/E_2) on the first three natural frequencies of a cantilever composite I-beam under axial compressive force and tensile force with value $(0.5\overline{P}_{cr})$ are investigated. The stacking sequence of the flanges and web are $[0/90]_s$, (Fig.**??**c). For this lay-up, all the coupling stiffnesses vanish and thus, the three distinct vibration mode, flexural vibration in the x- and y-direction and torsional vibration are identified. It is observed from Fig.**??** that the natural frequencies $\omega_{x_1}, \omega_{\theta_1}$ and ω_{y_1} increase with increasing orthotropy (E_1/E_2) for two cases considered.

8. CONCLUDING REMARKS

A analytical model based on shear-deformable beam theory is developed to study free vibration of axially loaded thin-walled composite Timoshenko beams with arbitrary lay-ups. This model is capable of predicting accurately the natural frequencies, load-frequency interaction curves as well as corresponding vibration mode shapes for various configuration. All of the possible vibration mode shapes including the flexural mode in the x- and y-direction, the

torsional mode, and fully coupled flexural-torsional-shearing mode are included in the analysis. The shear effects become significant for lower span-to-height ratio. The present model is found to be appropriate and efficient in analyzing free vibration problem of axially loaded thin-walled composite Timoshenko beams.

Acknowledgments

This research was supported by Basic Research Laboratory Program of the National Research Foundation of Korea (NRF) funded by the Ministry of Education, Science and Technology through NRF2010-0019373, and by Korea Ministry of Knowledge Economy under the national HRD support program for convergence information technology supervised by National IT Industry Promotion Agency through NIPA-2010-C6150-1001-0013. The authors also would like to thank the anonymous reviewers for their suggestions in improving the standard of the manuscript.

References

Vlasov, V. Z. (1961) *Thin Walled Elastic Beams*. Israel Program for Scientific Transactions, Jerusalem.

Gjelsvik, A. (1981) *The theory of thin walled bars*. Wiley, New York.

Bleich, F., Ramsey, L., and Bleich, H. (1952) *Buckling strength of metal structures*. McGraw-Hill, New York.

Timoshenko, S. and Gere, J. M. (1961) *Theory of elastic stability*. McGraw-Hill, New York.

Timoshenko, S., Young, D. H., and Weaver, W. J. R. (1974) *Vibration problems in engineering*. John Wiley & Sons, New York.

Bank, L. C. and Kao, C. (1990) Dynamic Response of Thin-Walled Composite Material Timoshenko Beams. *J Energ Resour*, **112**, 149–154.

Cortinez, V. H. and Piovan, M. T. (2002) Vibration and buckling of composite thin-walled beams with shear deformability. *J Sound Vib*, **258**, 701 – 723.

Machado, S. P. and Cortinez, V. H. (2007) Free vibration of thin-walled composite beams with static initial stresses and deformations. *Eng Struct*, **29**, 372 – 382.

Banerjee, J. R. and Williams, F. W. (1996) Exact dynamic stiffness matrix for composite Timoshenko beams with applications. *J Sound Vib*, **194**, 573 – 585.

Banerjee, J. R. (1998) Free vibration of axially loaded composite Timoshenko beams using the dynamic stiffness matrix method. *Comput Struct*, **69**, 197 – 208.

Banerjee, J. R., Su, H., and Jayatunga, C. (2008) A dynamic stiffness element for free vibration analysis of composite beams and its application to aircraft wings. *Comput Struct*, **86**, 573 – 579.

Li, J., Shen, R., Hua, H., and Xianding, J. (2004) Bending-torsional coupled dynamic response of axially loaded composite Timosenko thin-walled beam with closed cross-section. *Compos Struct*, **64**, 23 – 35.

Li, J., Wu, G., Shen, R., and Hua, H. (2005) Stochastic bending-torsion coupled response of axially loaded slender composite-thin-walled beams with closed cross-sections. *Int J Mech Sci*, **47**, 134 – 155.

Kaya, M. and Ozgumus, O. O. (2007) Flexural-torsional-coupled vibration analysis of axially loaded closed-section composite Timoshenko beam by using DTM. *J Sound Vib*, **306**, 495 – 506.

Kim, N. I., Shin, D. K., and Park, Y. S. (2008) Dynamic stiffness matrix of thin-walled composite I-beam with symmetric and arbitrary laminations. *J Sound Vib*, **318**, 364 – 388.

Kim, N. I. and Shin, D. K. (2009) Dynamic stiffness matrix for flexural-torsional, lateral buckling and free vibration analyses of mono-symmetric thin-walled composite beams. *Int J Struct Stab Dy*, **9**, 411–436.

Lee, J. (2005) Flexural analysis of thin-walled composite beams using shear-deformable beam theory. *Compos Struct*, **70**, 212 – 222.

Vo, T. P. and Lee, J. (2009) On sixfold coupled buckling of thin-walled composite beams. *Compos Struct*, **90**, 295 – 303.

Vo, T. P., Lee, J., and Ahn, N. (2009) On sixfold coupled vibrations of thin-walled composite box beams. *Compos Struct*, **89**, 524 – 535.

Jones, R. M. (1999) *Mechanics of Composite Materials*. Taylor & Francis.

Vo, T. P. and Lee, J. (2010) On triply coupled vibrations of axially loaded thin-walled composite beams. *Comput Struct*, **88**, 144–153.

CAPTIONS OF TABLES

Table **??**: Critical bucking loads (N) of a cantilever mono-symmetric composite I-beam with symmetric angle-ply laminates $[\pm\theta]_{4s}$ in the flanges and web.

Table **??**: Effect of axial force on the first four natural frequencies (Hz) of a cantilever mono-symmetric composite I-beam with symmetric angle-ply laminates $[\pm\theta]_{4s}$ in the flanges and web under constant axial forces at the centroid (( ): natural frequency with an axial compressive force, [ ]: natural frequency with an axial tensile force).

Table **??**: Effect of axial force on the first four natural frequencies with respect to the fiber angle change in the flanges and web of a simply supported composite beam.

Table **??**: Effect of axial force on the first four natural frequencies with respect to the fiber angle change in the bottom flange of a clamped composite beam.

CAPTIONS OF FIGURES

Figure **??**: Definition of coordinates and generalized displacements in thin-walled open sections.

Figure **??**: Geometry and stacking sequences of thin-walled composite I-beam.

Figure **??**: The first four normal mode shapes of the flexural, torsional and corresponding shearing components with the fiber angle 30° in the flanges and web of a simply supported composite beam under an axial compressive force ($\overline{P} = 0.5\overline{P}_{cr}$).

Figure **??**: Three dimensional interaction diagram between between axial force and the first four natural frequencies with respect to the fiber angle change in the flanges and web of a simply supported composite beam.

Figure **??**: Effect of axial force on the first four natural frequencies with the fiber angle 0° in the flanges and web of a simply supported composite beam.

Figure **??**: Effect of axial force on the first four natural frequencies with the fiber angle 30° in the flanges and web of a simply supported composite beam.

Figure **??**: Effect of axial force on the first four natural frequencies with the fiber angle 60° in the flanges and web of a simply supported composite beam.

Figure **??**: Effect of axial force on the first four natural frequencies with the fiber angle 0° in the bottom flange of a clamped composite beam.

Figure **??**: Effect of axial force on the first four natural frequencies with the fiber angle 60° in the bottom flange of a clamped composite beam.

Figure **??**: The first four normal mode shapes of the flexural, torsional and corresponding shearing components with the fiber angle 30° in the bottom flange of a clamped composite beam under an axial compressive force ($\overline{P} = 0.5\overline{P}_{cr}$).

Figure **??**: Variation of the first three natural frequencies with respect to modulus ratio change of a cantilever composite beam under an axial compressive force ($\overline{P} = 0.5\overline{P}_{cr}$) and an axial tensile force ($\overline{P} = -0.5\overline{P}_{cr}$).

TABLE 1 Critical bucking loads (N) of a cantilever mono-symmetric composite I-beam with symmetric angle-ply laminates $[\pm\theta]_{4s}$ in the flanges and web.

Lay-ups	Kim and Shin [**?**]		Present
	ABAQUS	Analytical	
$[0]_{16}$	2969.7	2998.1	2993.2
$[15/-15]_{4s}$	2790.9	2813.8	2803.6
$[30/-30]_{4s}$	2190.6	2201.1	2184.7
$[45/-45]_{4s}$	1558.9	1562.4	1546.0
$[60/-60]_{4s}$	1239.4	1241.5	1277.8
$[75/-75]_{4s}$	1132.2	1134.5	1126.7

TABLE 2 Effect of axial force on the first four natural frequencies (Hz) of a cantilever mono-symmetric composite I-beam with symmetric angle-ply laminates $[\pm\theta]_{4s}$ in the flanges and web under constant axial forces at the centroid (( ): natural frequency with an axial compressive force, [ ]: natural frequency with an axial tensile force).

Mode	Stacking sequences and values of axial force											
	$[0]_{16}$		$[15/-15]_{4s}$		$[30/-30]_{4s}$		$[45/-45]_{4s}$		$[60/-60]_{4s}$		$[75/-75]_{4s}$	
	P_0=1499.05 N		P_0=1406.90 N		P_0=1100.55 N		P_0=781.20 N		P_0=620.75 N		P_0=567.25 N	
	Ref. [**?**]	Present	Ref. [**?**]	Present	Ref. [**?**]	Present	Ref. [**?**]	Present	Ref. [**?**]	Present	Ref. [**?**]	Present
1	(19.087)	(19.049)	(18.505)	(18.433)	(16.401)	(16.273)	(13.841)	(13.686)	(12.342)	(12.196)	(11.791)	(11.705)
	26.295	26.258	25.508	25.449	22.641	22.538	19.130	19.003	17.063	16.942	16.294	16.223
	[31.498]	[31.457]	[30.568]	[30.509]	[27.162]	[27.062]	[22.970]	[22.844]	[20.492]	[20.371]	[19.561]	[19.491]
2	(43.267)	(43.140)	(44.524)	(44.262)	(46.335)	(45.047)	(40.135)	(40.011)	(35.692)	(35.585)	(34.273)	(34.160)
	46.472	46.335	47.346	47.091	48.325	47.100	42.243	42.115	37.575	37.465	36.066	35.949
	[49.414]	[49.268]	[49.969]	[49.716]	[50.213]	[49.042]	[44.224]	[44.091]	[39.345]	[39.231]	[37.751]	[37.630]
3	(59.242)	(58.864)	(56.205)	(55.895)	(48.304)	(48.110	(45.879)	(42.703)	(42.648)	(39.083)	(37.990)	(36.413)
	61.988	61.600	58.920	58.600	50.772	50.572	47.267	44.199	43.831	40.377	39.210	37.687
	[64.586]	[64.185]	[61.484]	[61.152]	[53.096]	[52.889]	[48.593]	[45.626]	[44.963]	[41.612]	[40.374]	[38.902]
4	(129.73)	(129.088)	(127.28)	(126.499)	(118.02)	(116.392)	(104.11)	(101.485)	(93.778)	(91.117)	(88.027)	(86.615)
	138.17	137.528	135.30	134.535	124.68	123.143	109.44	106.946	98.472	95.946	92.605	91.261
	[146.02]	[145.376]	[142.77]	[142.020]	[130.94]	[129.469]	[114.47]	[112.091]	[102.92]	[100.501]	[96.927]	[95.640]

TABLE 3 Effect of axial force on the first four natural frequencies with respect to the fiber angle change in the flanges and web of a simply supported composite beam.

Fiber	Buckling	Axial force	Uncoupled solution				Coupled solution			
angle	loads ($\overline{P}_{cr}$)	$\overline{P}$	w_{x_1}	w_{θ_1}	w_{y_1}	w_{x_2}	w_1	w_2	w_3	w_4
0	11.214		4.866	5.885	15.023	22.687	4.866	5.885	15.023	22.687
30	3.290	$0.5\overline{P}_{cr}$	2.635	3.379	10.000	13.691	2.635	3.333	9.994	13.690
60	0.602	(compression)	1.127	1.520	4.397	5.914	1.127	1.515	4.396	5.914
90	0.486		1.012	1.345	3.951	5.311	1.012	1.345	3.951	5.311
0	11.214		6.881	7.635	15.789	24.680	6.881	7.635	15.788	24.680
30	3.290	0	3.727	4.285	10.337	14.665	3.727	4.249	10.332	14.664
60	0.602	(no axial force)	1.594	1.892	4.537	6.326	1.594	1.888	4.536	6.326
90	0.486		1.432	1.683	4.077	5.682	1.432	1.683	4.077	5.682
0	11.214		8.427	9.053	16.518	26.524	8.427	9.053	16.518	26.524
30	3.290	$-0.5\overline{P}_{cr}$	4.565	5.030	10.664	15.578	4.564	4.999	10.660	15.577
60	0.602	(tension)	1.952	2.202	4.673	6.714	1.952	2.199	4.672	6.713
90	0.486		1.753	1.964	4.199	6.030	1.753	1.964	4.199	6.030

TABLE 4 Effect of axial force on the first four natural frequencies with respect to the fiber angle change in the bottom flange of a clamped composite beam.

Fiber	Buckling	Axial force	No shear ([**?**])				Present			
angle	loads ($\overline{P}_{cr}$)	$\overline{P}$	w_1	w_2	w_3	w_4	w_1	w_2	w_3	w_4
0	29.582		10.477	12.438	33.759	38.188	8.370	10.509	21.035	24.770
30	15.918	$0.5\overline{P}_{cr}$	6.965	9.433	23.078	28.958	6.183	9.444	17.690	20.444
60	2.861	(compression)	2.858	9.481	9.524	19.879	2.725	8.965	11.192	18.145
90	2.290		2.558	8.517	9.491	17.773	2.449	8.050	11.293	16.480
0	29.582		13.734	15.277	37.850	39.199	11.564	14.252	22.527	29.090
30	15.918	0	9.540	11.458	26.275	30.448	8.646	11.836	19.009	23.219
60	2.861	(no axial force)	3.975	9.871	10.911	21.351	3.805	10.305	11.753	18.325
90	2.290		3.557	9.758	9.805	19.091	3.422	9.258	11.748	17.767
0	-29.582		16.306	17.628	40.180	41.516	13.957	17.094	23.913	32.762
30	-15.918	$-0.5\overline{P}_{cr}$	11.512	13.151	29.100	31.129	10.495	13.767	20.038	25.815
60	-2.861	(tension)	4.823	10.246	12.131	22.725	4.612	11.472	12.287	18.502
90	-2.290		4.315	10.107	10.850	20.321	4.149	10.310	12.185	18.364

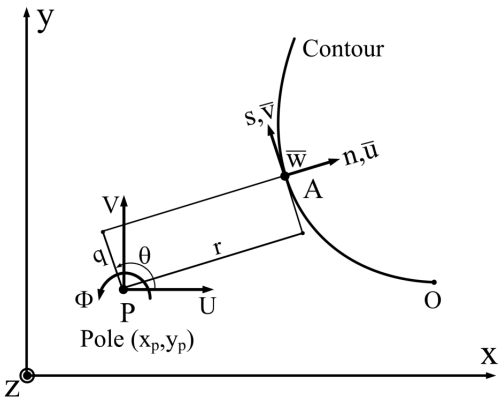

FIG. 1 Definition of coordinates in thin-walled open sections.

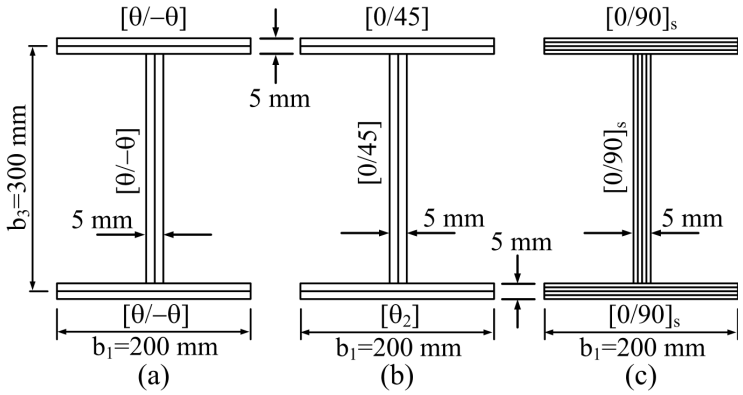

FIG. 2 Geometry and stacking sequences of thin-walled composite I-beam.

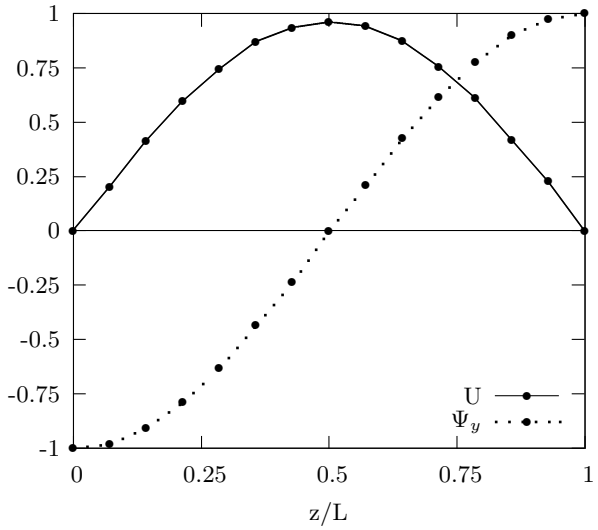

(a) Mode 1

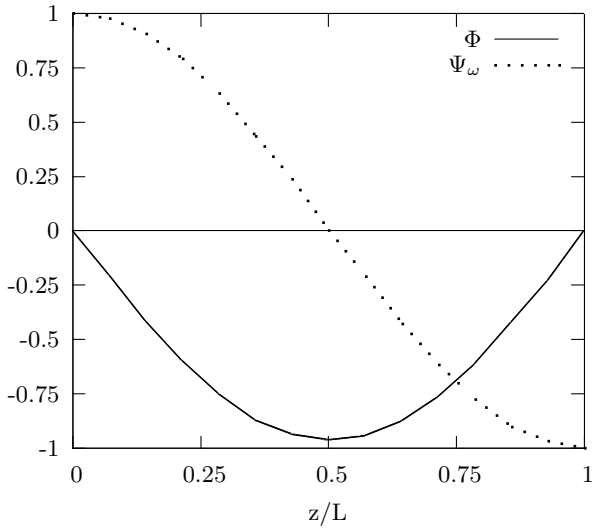

(b) Mode 2

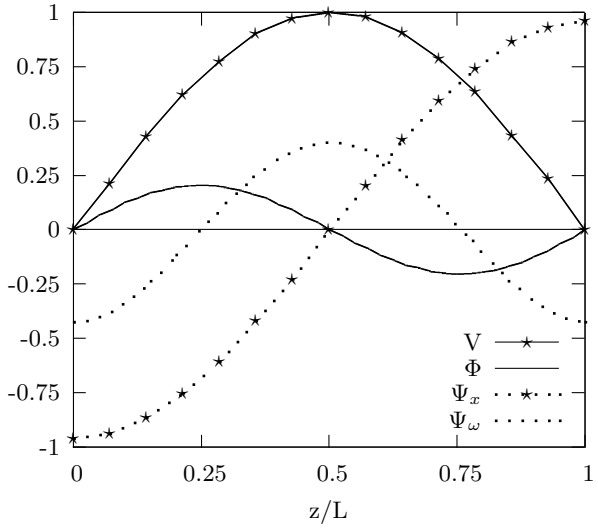

(c) Mode 3

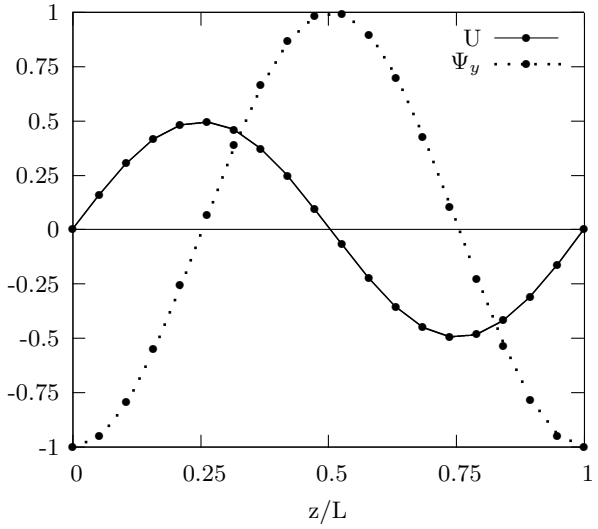

(d) Mode 4

FIG. 3 The first four normal mode shapes of the flexural, torsional and corresponding shearing components with the fiber angle 30° in the flanges and web of a simply supported composite beam under an axial compressive force ($\overline{P} = 0.5\overline{P}_{cr}$).

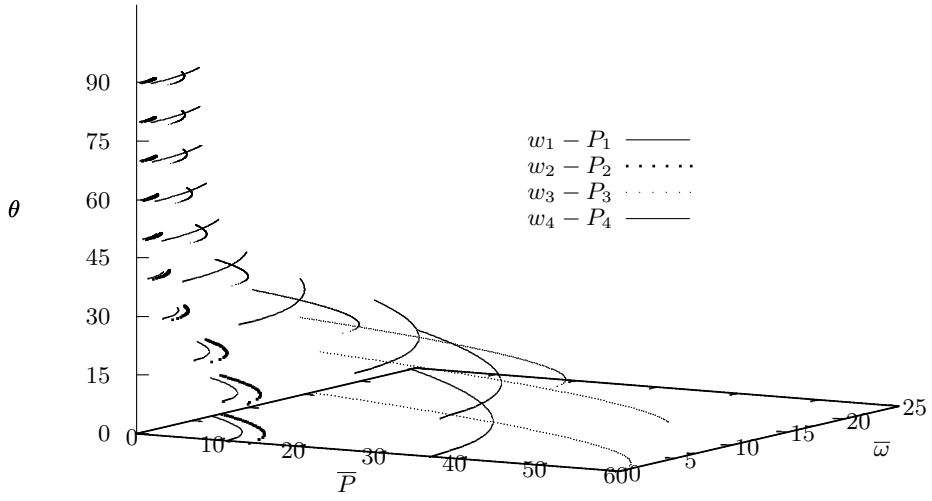

FIG. 4 Three dimensional interaction diagram between between axial force and the first four natural frequencies with respect to the fiber angle change in the flanges and web of a simply supported composite beam.

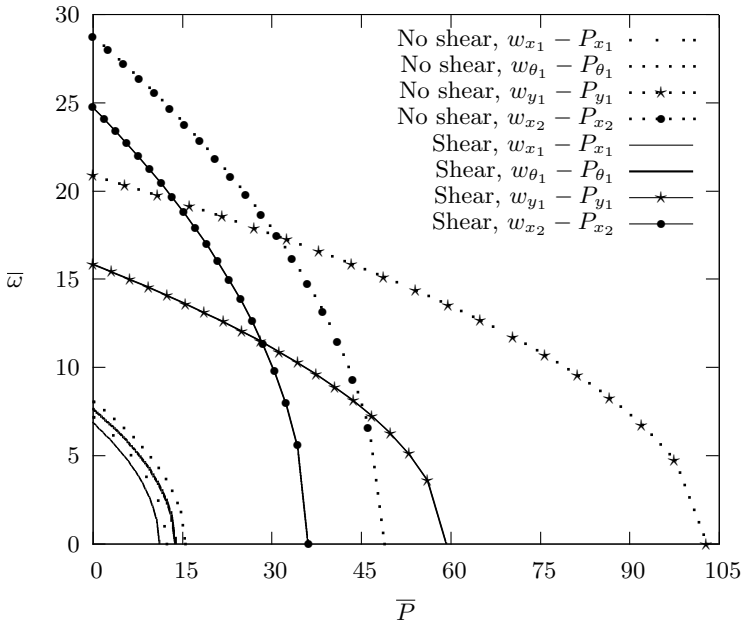

FIG. 5 Effect of axial force on the first four natural frequencies with the fiber angle 0° in the flanges and web of a simply supported composite beam.

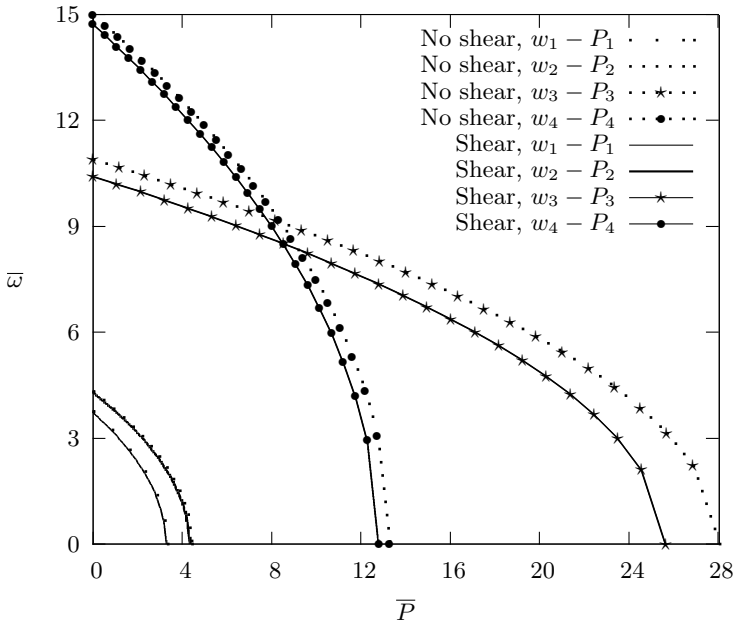

FIG. 6 Effect of axial force on the first four natural frequencies with the fiber angle 30° in the flanges and web of a simply supported composite beam.

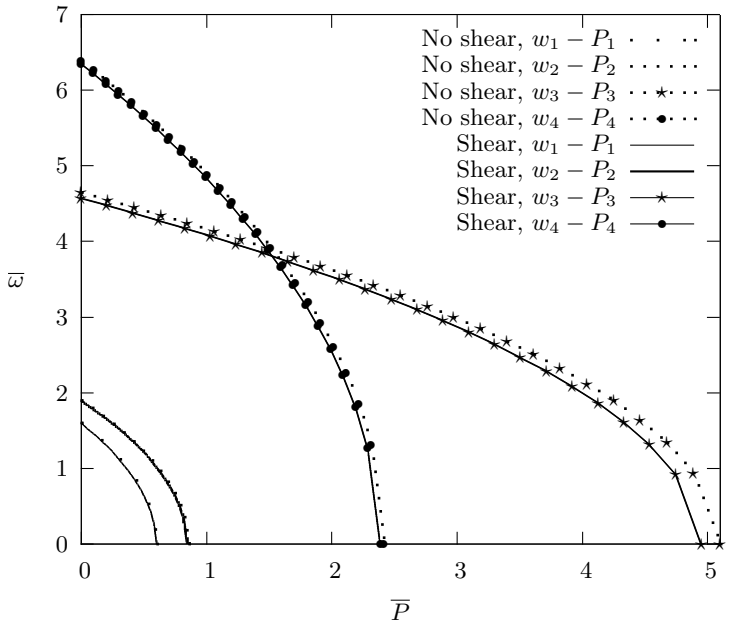

FIG. 7 Effect of axial force on the first four natural frequencies with the fiber angle 60° in the flanges and web of a simply supported composite beam.

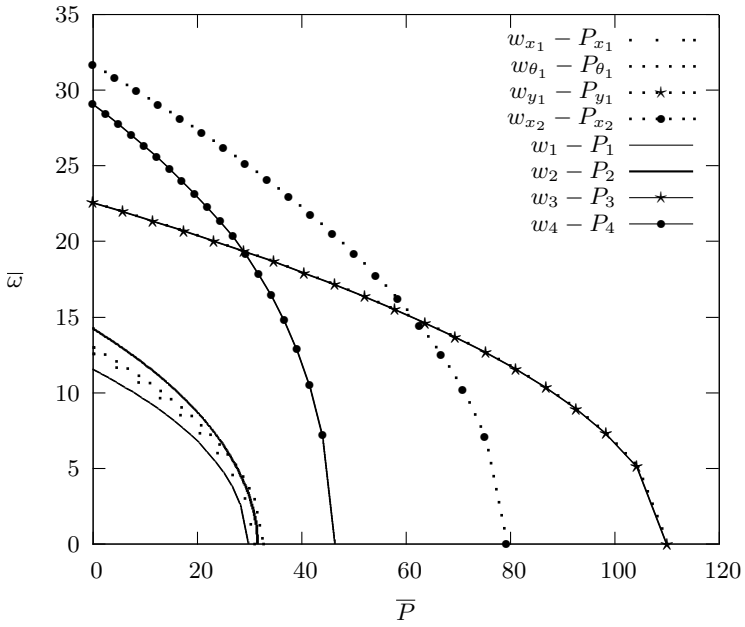

FIG. 8 Effect of axial force on the first four natural frequencies with the fiber angle 0° in the bottom flange of a clamped composite beam.

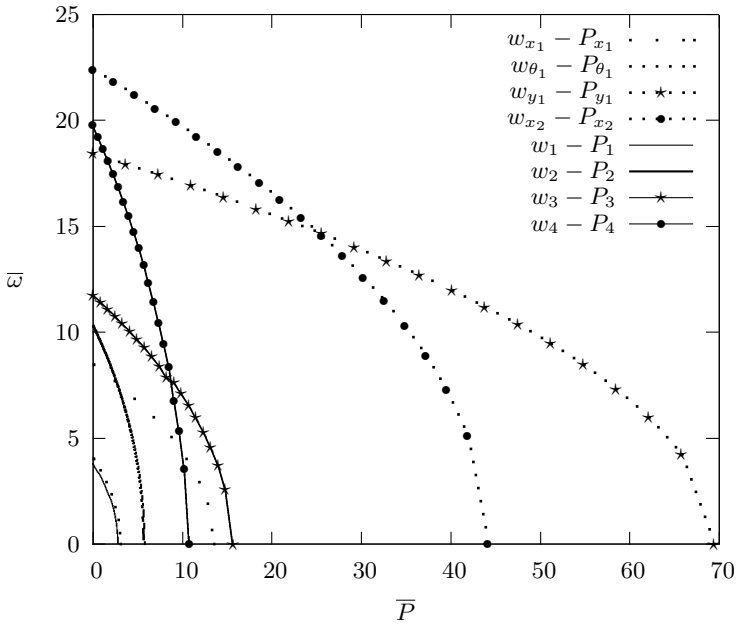

FIG. 9 Effect of axial force on the first four natural frequencies with the fiber angle 60° in the bottom flange of a clamped composite beam.

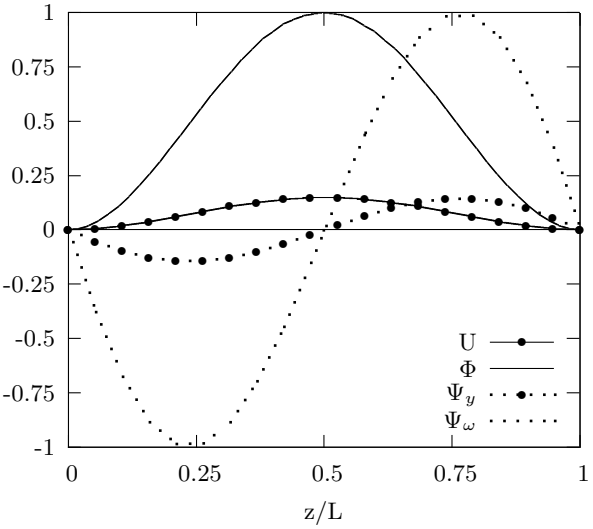

(a) Mode 1

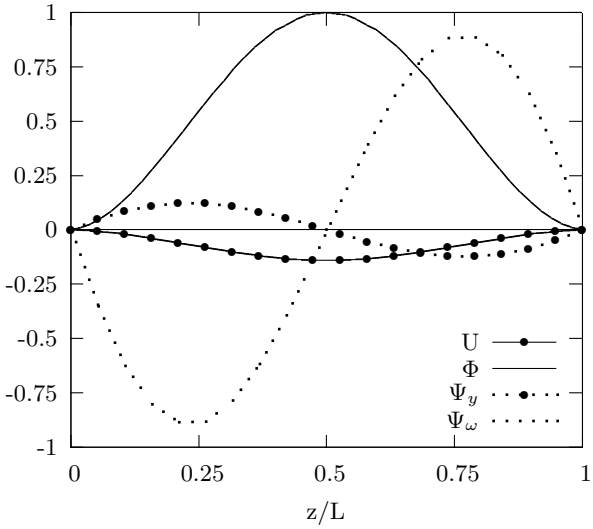

(b) Mode 2

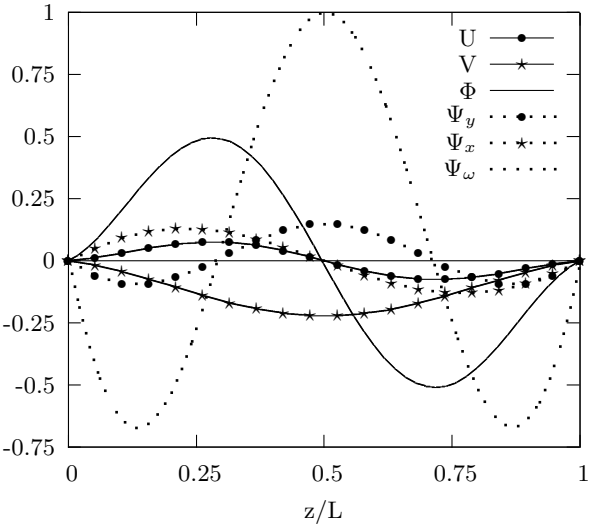

(c) Mode 3

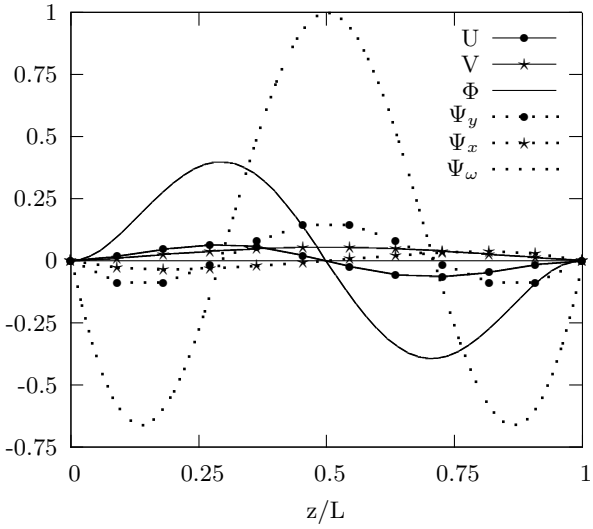

(d) Mode 4

FIG. 10 The first four normal mode shapes of the flexural, torsional and corresponding shearing components with the fiber angle 30° in the bottom flange of a clamped composite beam under an axial compressive force ($\overline{P} = 0.5\overline{P}_{cr}$).

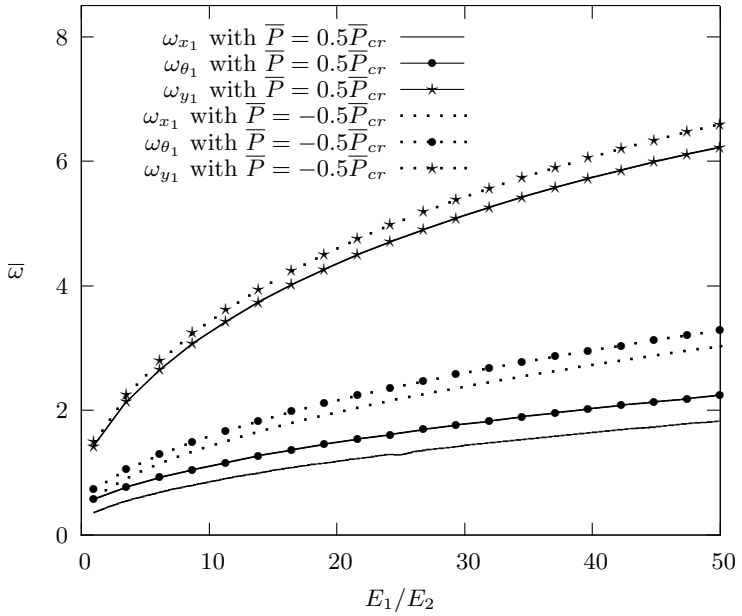

FIG. 11 Variation of the first three natural frequencies with respect to modulus ratio change of a cantilever composite beam under an axial compressive force ($\overline{P} = 0.5\overline{P}_{cr}$) and an axial tensile force ($\overline{P} = -0.5\overline{P}_{cr}$).